References and Notes

1. S. M. Marshall and T. A. Stephenson, *Sci. Rep. Great Barrier Reef Exped. 1928–1929* **3**, 219 (1933).
2. L. H. Hyman, *The Invertebrates*, vol. 1, *Protozoa through Ctenophora* (McGraw-Hill, New York, 1940).
3. T. W. Vaughan and J. W. Wells, *Geol. Soc. Am. Spec. Pap.* **44**, 1 (1943).
4. N. Abe, *Palao Trop. Biol. Sta. Stud.* **1**, 73 (1937).
5. K. Atoda, *Sci. Rep. Res. Inst. Tohoku Univ. Ser. D* **20**, 105 (1953).
6. J. Harrigan, thesis, University of Hawaii (1972).
7. J. B. Lewis, *J. Exp. Mar. Biol. Ecol.* **15**, 165 (1974).
8. J. S. Stimpson, *Mar. Biol.* **48**, 173 (1978).
9. B. Rinkevich and Y. Loya, *Mar. Ecol. Prog. Ser.* **1**, 133 (1979).
10. ———, *ibid.*, p. 145.
11. A. Szmant-Froelich *et al.*, *Biol. Bull. (Woods Hole, Mass.)* **158**, 257 (1980).
12. B. L. Kojis and N. J. Quinn, *Bull. Mar. Sci.* **31**, 558 (1981).
13. ———, *Proceedings of the 4th International Coral Reef Symposium, Manila, Philippines* **2**, 145 (1981).
14. B. L. Kojis and N. J. Quinn, *Mar. Ecol. Prog. Ser.* **8**, 251 (1982).
15. A. M. Bothwell, *Proceedings of the 4th International Coral Reef Symposium, Manila, Philippines* **2**, 137 (1981).
16. P. R. G. Tranter, D. N. Nicholson, D. Kinchington, *J. Mar. Biol. Assoc. U.K.* **62**, 845 (1982).
17. Y. H. Fadlallah, *Oecologia (Berlin)* **55**, 379 (1982).
18. V. J. Harriott, *Coral Reefs*, in press.
19. Of the 32 species in Table 1, 22 species were regularly sampled and showed no evidence of a second gametogenic cycle throughout the year. Four species of *Turbinaria* were also regularly sampled to determine that they had an annual gametogenic cycle and a single spawning season.
20. R. H. Richmond and P. L. Jokiel, *Bull. Mar. Sci.*, in press.
21. A. C. Giese and J. S. Pearse, in *Reproduction of Marine Invertebrates*, A. C. Giese and J. S. Pearse, Eds. (Academic Press, New York, 1974), vol. 1, pp. 2–49.
22. P. Korringa, *Geol. Soc. Am.* **67**, 917 (1957).
23. R. D. Campbell, in *Reproduction of Marine Invertebrates*, A. C. Giese and J. S. Pearse, Eds. (Academic Press, New York, 1974), vol. 1, pp. 133–199.
24. This was determined by extensive sampling (more than 20 colonies) for 9 species (6 *Acropora*, 2 *Goniastrea*, and 1 *Platygyra*). In a further 11 species, random samples were taken after the spawning event to verify the absence of eggs throughout the population. This was also confirmed for a population of *Montipora ramosa* by A. Heyward (personal communication).
25. R. L. Miller, in *Advances in Invertebrate Reproduction*, W. H. Clark and T. S. Adams, Eds. (Elsevier/North-Holland, New York, 1980), pp. 289–317.
26. T. J. Done, *Coral Reefs* **1**, 95 (1982).
27. R. W. Grigg, *Pac. Sci.* **35**, 15 (1981).

28. We thank J. D. Collins for assistance with fieldwork in 1982. C. G. Alexander, J. S. Lucas, J. R. Ottaway, M. M. Pichon, V. J. Harriott, B. A. Harrison, and D. G. Reid made valuable comments upon the manuscript. We also thank P. Watson of Shark World, Nelly Bay, Magnetic Island, for his cooperation and logistic support in 1981. Funded in part by a grant from the Great Barrier Reef Marine Park Authority in 1981, and an MSTGS grant to C.C.W.

5 July 1983; accepted 1 November 1983

Phenylalanine Transfer RNA: Molecular Dynamics Simulation

Abstract. *Yeast phenylalanine transfer RNA was subjected to a 12-picosecond molecular dynamics simulation. The principal features of the x-ray crystallographic analysis are reproduced, and the amplitudes of atomic displacements appear to be determined by the degree of exposure of the atoms. An analysis of the hydrogen bonds shows a correlation between the average length of a bond and the fluctuation in that length and reveals a rocking motion of bases in Watson-Crick guanine · cytosine base pairs. The in-plane motions of the bases are generally of larger amplitude than the out-of-plane motions, and there are correlations in the motions of adjacent bases.*

Computer simulations with the molecular dynamics algorithm have been used to investigate intramolecular motions in proteins on the picosecond time scale (*1, 2*), and Levitt has recently reported the first simulation for DNA (*3*). He found that, when he included the partial atomic charges, the double helix unwound; to preserve the tertiary structure he had to set all of the partial charges to zero. We describe the first successful molecular dynamics simulation for a transfer RNA (tRNA). By careful equilibration of the structure, we have been able to include full electrostatic effects (*4*); a similar result for a DNA simulation has just been reported (*5*).

As in our previous conformational energy study (*6*) on large-scale bending in phenylalanine transfer RNA ($tRNA^{Phe}$), we began with the 2.5-Å crystal structure (*7*) and used standard parameters (*8–10*) for the potential energy functions. Partial atomic charges (*11*) have been included, and a distance-dependent dielectric constant was used to mimic solvent dielectric effects (*12*). No counterions were included, but their effect was approximated by scaling charges on atoms in phosphate groups to give a net charge of 0.2 electron per nucleotide. Explicit hydrogen atoms are not included, and extended atoms represent each heavy atom and the hydrogens covalently bound to it (*12*); hydrogen bond lengths thus refer to the distance between the heavy atoms of the donor and acceptor groups. A normal van der Waals potential function (*4*) was used in this simulation.

The structure was subjected to 100 cycles of steepest descent energy minimization, after which atomic velocities were assigned with a Maxwellian distribution corresponding to a temperature of 50 K, and the molecule was warmed by velocity reassignments at 1-picosecond intervals with temperatures rising to 300 K at 11 psec. This temperature was reassigned at 0.2-psec intervals over a period of 5 psec, and equilibration was completed by a 4 psec free run. Data analysis covered the interval from 20 to 32 psec, during which time the average temperature of the molecule was 303.7 K.

The integrity of protein structures during molecular dynamics experiments may be partly due to their compact and globular shapes and to the fact that the simulations are generally done near the isoelectric point. In view of the extended structure and net charge of $tRNA^{Phe}$, and because of the difficulties (described above) that Levitt encountered with structural degradation in his DNA simulation (*3*), we have examined several structural parameters to verify that our model of $tRNA^{Phe}$ does remain intact. To begin with, a visual inspection of computer graphics pictures of representative structures from the trajectory showed that the overall structure is preserved. The radius of gyration is 23.4 Å in the crystal structure (*7*), while it varies about a mean value of 22.7 Å with an amplitude of 0.5 Å and an apparent period of about 10 psec in the simulation (*4*). Since there is no solvent in the stimulation, so that there are no attractive forces between atoms on the surface of the molecule and the solvent, the 3 percent shrinkage of the model with respect to the crystal is not surprising. The oscillation in the radius of gyration reflects a concerted bending motion, a collective motion of small amplitude but extending over the entire molecule: the angle between the two arms oscillates with an amplitude of about 1°, and the distance between the anticodon and the acceptor terminus oscillates with an amplitude of about 1 Å. This motion is reminiscent of the hinge-bending mode proposed by others (*13, 14*) and examined in our earlier study (*6*).

More critical measures of the preservation of the structure are provided by an examination of the ribose puckers and of some of the parameters of the helix. We have calculated the puckering angle (*15*) for all 76 sugar moieties over the course of the trajectory, and we find that 65 of them are in the conformational energy valley near the C3′-*endo* configuration, and 11 are C2′-*endo*, exactly as in the crystal. Although the puckering angles oscillate about these two local minima, none of the sugars changes from C3′-*endo* to C2′-*endo* or vice versa. Helix integrity is demonstrated by the interphosphate distances, the twist angles of successive base pairs, and the orientation of base plane normal vectors, all of which also have average values near those of the crystal structure.

The root-mean-square deviations of

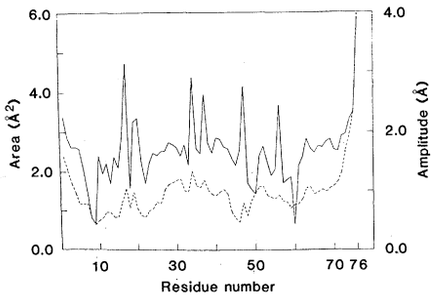

Fig. 1. Comparison of root-mean-square atomic displacements (broken line and scale at right) and solvent-accessible surface contact area (solid line and scale at left) for the 76 residues of $tRNA^{Phe}$. Surface areas were calculated with the use of the algorithm of Lee and Richards (*20*) with a spherical probe radius of 1.4 Å.

the atomic positions about their mean values, which represent the amplitudes of the thermal motions, are of the same magnitude as those reported for bovine pancreatic trypsin inhibitor (*16, 17*) and for ferrocytochrome c (*18*). The root-mean-square vibrational amplitudes for each residue are shown in Fig. 1. There is a general trend of larger motions near the ends of the arms (residues 1 to 3 and 70 to 76 in the acceptor stem and residues 32 to 38 in the anticodon loop) and smaller motions near the center of the molecule (residues 7 to 16, 48 to 50, and 59 to 61), in accordance with the crystallographic studies (*19*). Superimposed on this general trend is a series of peaks and valleys that are explained by examining the average solvent-accessible surface contact area of each residue (*20*). The vibrational amplitudes are highly correlated with residue exposure (Fig. 1), a reflection of the influence of packing restrictions on atomic motion. When we consider the atomic motions within a single residue, they are generally largest for the phosphate atoms, intermediate for those of the ribose, and smallest for those of the base, again in agreement with the thermal factors derived from the crystal structure (*19*).

Two interesting dynamic features of the hydrogen bonds have revealed themselves. The first of these, the correlation between the average length of a hydrogen bond and the amplitude of the thermal fluctuations in the bond length, is shown in Fig. 2. While it is not surprising that the bonds associated with secondary structure are generally shorter and stiffer than those of the tertiary structure, the correlation between bond length and bond stiffness is striking. The relaxation times for these motions are on the order of 0.1 psec. The second feature was discovered early in our search for collective motions in the double-helical regions and is summarized by the correlation coefficients for pairs of hydrogen bonds (Table 1). These coefficients were calculated because it was to be expected that the lengths of the Watson-Crick hydrogen bonds within a given base pair should be highly correlated as the bases move toward and away from one another. This is confirmed by the positive coefficients for bonds in adenine · uracil (AU) pairs and for neighboring bonds in guanine · cytosine (GC) pairs. The unexpected result is the collection of negative correlation coefficients for bonds 1 and 3 in GC pairs, revealing a rocking motion of the bases, with one bond growing longer as the other is shortened. Most of these coefficients appear statistically significant ($r_{crit} = 0.053$; $P < 0.01$; d.f. = 2399), but such a test is suspect when applied to a single coefficient that is derived from a sequence of structures that are not independent of one another. A more stringent test is the simple sign test, which gives a highly statistically significant result ($P < 0.01$) when applied to the whole set of coefficients which represent GC rocking (r_{13}), demonstrating unambiguously the occurrence of these rocking motions.

We have also begun to analyze the base motions. As would be expected, the in-plane motions (transverse to the helix axis) are generally larger than the out-of-plane (longitudinal) motions. Interestingly, the largest ratio for transverse to longitudinal motions is found in the three bases of the anticodon, which are not in a double helical region. There are also substantial correlations in both the longitudinal and transverse motions of stacked bases; within a base pair, the transverse motions are generally more strongly coupled than motions along the helix axis.

Table 1. Correlation coefficients for lengths of hydrogen bonds. The correlation coefficient between the lengths of bonds i and j is designated r_{ij}. For AU base pairs and the pair G4–U69, there are only two hydrogen bonds. In GC base pairs, bond 2 refers to the middle of the three Watson-Crick bonds, from N1(G) to N3(C), while bond 1 is from N4(C) to O6(G) and bond 3 is from N2(G) to O2(C).

Base pair	r_{12}	r_{23}	r_{13}
	Acceptor stem		
G1–C72	0.56	0.51	0.04
C2–G71	0.55	0.30	−0.07
G3–C70	0.43	0.17	−0.28
G4–U69	0.20		
A5–U68	0.35		
U6–A67	0.08		
U7–A66	0.33		
	D stem		
m^2G10–C25	0.07	0.70	−0.14
C11–G24	0.36	0.27	−0.17
U12–A23	−0.23		
C13–G22	0.19	0.22	−0.10
	Anticodon stem		
C27–G43	0.37	0.65	−0.01
C28–G42	0.33	0.22	−0.10
A29–U41	0.19		
G30–m^5C40	0.34	0.29	−0.13
A31–ψ39	0.26		
	T stem		
m^5C49–G65	0.24	0.30	−0.23
U50–A64	0.18		
G51–C63	0.46	0.39	−0.18
U52–A62	0.29		
G53–C61	0.24	0.40	−0.10

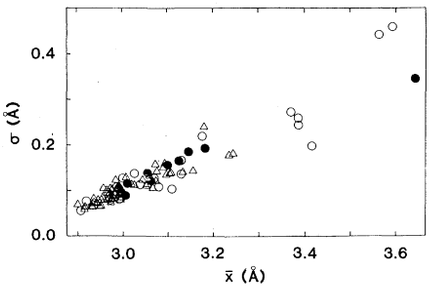

Fig. 2. Correlation between the mean length of the hydrogen bonds ($\bar{x}$) and root-mean-square fluctuation in bond length (σ). Secondary structure hydrogen bonds are represented by triangles, while those of the tertiary structure are represented by circles. Closed circles indicate bonds between O2′ hydroxyls of one ribose and oxygen atoms (O4′ or O5′) of the succeeding residue, while open circles indicate other tertiary hydrogen bonds. Distances are between donor and acceptor group heavy atoms.

The molecular dynamics simulation of $tRNA^{Phe}$ is thus seen to reveal a variety of motions over a broad range of time scales. Extending the simulation to a longer time interval should lead to a fuller characterization of the slow, large-scale motions and the relationships between those and the rapid, local motions.

STEPHEN C. HARVEY
M. PRABHAKARAN
Department of Biochemistry, University of Alabama in Birmingham, Birmingham 35294
BORYEU MAO
J. ANDREW MCCAMMON
Department of Chemistry, University of Houston, Houston, Texas 77004

References and Notes

1. J. A. McCammon and M. Karplus, *Annu. Rev. Phys. Chem.* **31**, 29 (1980).
2. M. Karplus and J. A. McCammon, *CRC Crit. Rev. Biochem.* **9**, 293 (1981).
3. M. Levitt, *Cold Spring Harbor Symp. Quant. Biol.* **47**, 251 (1983).
4. M. Prabhakaran, S. C. Harvey, B. Mao, J. A. McCammon, *J. Biomol. Struct. Dyn.* **1**, 357 (1983).
5. B. Tidor, K. K. Irikura, B. R. Brooks, M. Karplus, *ibid.*, p. 231.
6. S. C. Harvey and J. A. McCammon, *Nature (London)* **294**, 286 (1981).
7. B. Hingerty, R. S. Brown, A. Jack, *J. Mol. Biol.* **124**, 523 (1978).
8. M. Levitt, *ibid.* **82**, 393 (1974).
9. ———, *Proc. Natl. Acad. Sci. U.S.A.* **75**, 640 (1978).
10. A. Jack, J. E. Ladner, A. Klug, *J. Mol. Biol.* **108**, 619 (1976).

11. K. J. Miller, *Biopolymers* **18**, 959 (1979).
12. J. A. McCammon, P. G. Wolynes, M. Karplus, *Biochemistry* **18**, 927 (1979).
13. J. D. Robertus *et al.*, *Nature (London)* **250**, 546 (1974).
14. T. Olson, M. J. Fournier, K. H. Langley, N. C. Ford, *J. Mol. Biol.* **102**, 193 (1976).
15. C. Altona and M. Sundaralingam, *J. Am. Chem. Soc.* **94**, 8205 (1972).
16. J. A. McCammon, B. R. Gelin, M. Karplus, *Nature (London)* **267**, 585 (1977).
17. M. Karplus and J. A. McCammon, *ibid.* **277**, 578 (1979).
18. S. H. Northrup, M. R. Pear, J. D. Morgan, J. A. McCammon, M. Karplus, *ibid.* **287**, 659 (1980).
19. J. L. Sussman, S. R. Holbrook, R. W. Warrant, G. M. Church, S. H. Kim, *J. Mol. Biol.* **123**, 607 (1978).
20. B. Lee and F. M. Richards, *ibid.* **55**, 379 (1971).
21. Supported by grants from the National Science Foundation to S.C.H. and J.A.M. The latter is an Alfred P. Sloan Fellow and recipient of Camille and Henry Dreyfus Teacher-Scholar and NIH Career Development awards.

7 July 1983; accepted 4 January 1984

Bioassay of Solubilized *Bacillus thuringiensis* var. *israelensis* Crystals by Attachment to Latex Beads

Abstract. *Solubilized crystals of* Bacillus thuringiensis *var.* israelensis *were 7000 times less toxic to* Aedes aegypti *larvae than intact crystals, presumably because mosquito larvae are filter feeders and selectively concentrate particles while excluding water and soluble molecules. A procedure is described whereby soluble toxins are adsorbed to 0.8-micrometer latex beads, with retention of toxicity. The latex bead assay should make it possible to analyze the structure and mode of action of the mosquito toxin.*

Control of several human diseases is based on controlling their mosquito or black fly vectors. Mosquitoes transmit such devastating diseases as malaria, encephalitis, yellow fever, dengue, and filariasis, while black flies transmit onchocerciasis. Biological control of these disease vectors has been made possible by the recent discovery of *Bacillus thuringiensis* var. *israelensis* (Bti). This bacterium produces a protein crystal during sporulation that is toxic to the larval stage of many mosquitoes and black flies. Purified particulate crystals are toxic to larvae of the mosquito *Aedes aegypti* at concentrations as low as 1 ng/ml (*1*). However, it has not been possible to determine the mode of action of the Bti toxin and the subunit of the multicomponent crystal (*1, 2*) containing the toxin. Larval toxicity disappears after the crystal is solubilized, probably because mosquito larvae, as filter feeders, selectively concentrate particles 0.5 to 10 μm in diameter while excluding water and soluble molecules (*3*).

We report here a procedure whereby potentially toxic soluble proteins are adsorbed to latex beads with retention of toxicity. The soluble toxin gains access to the larval gut because the particles to which it is attached are of the appropriate size to be concentrated during filter feeding. This procedure should prove effective for use with other soluble, gut-active compounds toxic to filter-feeding mosquito and black fly larvae and to net-making caddis flies, midges, and burrowing mayflies.

We confirmed that solubilized Bti proteins are still intrinsically toxic to mosquito larvae by adsorbing them to 0.8-μm latex beads (Table 1). The procedure was adapted from that described for the attachment of antibodies to latex beads (*4*). Bioassays were performed with second- to third-instar larvae of *A. aegypti* (*5*). The bead concentration was kept constant while the toxin concentration was varied through six or more dilutions covering the range from 100 to 0 percent mortality. Microscopic examination revealed larval guts gorged with ingested beads. The presence of excess beads minimized the effect of slight variations in larval number and size. Values of median lethal concentration (LC_{50}) were calculated after 4 hours instead of the more standard 24 hours because 4 hours approximates the larval transit time for nonnutritive particles in *Culex pipiens* (*6*) and because we wanted to avoid recycling of the beads. Values reported were calculated from three or more independent bioassays. Uncoated beads were not toxic to the larvae for at least 48 hours.

We confirmed that the solubilized Bti toxin was adsorbed by centrifuging the beads and washing them three times with 0.1*M* $NaPO_4$ buffer (*p*H 7.4) containing 0.01 percent polyvinylpyrrolidone. Larval toxicity remained constant even after repeated washings. The amount of toxin attached to the beads was determined by labeling the proteins with ^{125}I and measuring bead-adsorbed radioactivity after the attachment and centrifugation procedures (Fig. 1). The percentage of bead-attached proteins decreased from 80 to 45 percent as the protein concentration was increased from 2 to 37 μg/ml. However, there was no preferential attachment of individual proteins to the beads. Sodium dodecyl sulfate–polyacrylamide gel electrophoresis (SDS-PAGE) profiles of the solubilized proteins before and after attachment were virtually identical.

Further bioassays in the absence of beads showed that solubilized Bti crystals were about 7000 times less toxic than intact crystals (Table 1). When the solubilized proteins were adsorbed to latex beads of the appropriate size, the LC_{50} was reduced from 53,000 to 190 ng/ml, a 280-fold increase in toxicity. However, the LC_{50} for bead-attached toxin was still 25 times higher than that for intact crystals. This difference may reflect a decrease in toxicity on solubilization or an accumulation of physical factors due to the presence of the beads. Three possible physical factors are (i) decreased toxin ingestion due to the gut volume occupied by the beads and the longer transit time (*6*) caused by their nonnutritive status [merely mixing intact crystals with latex beads doubled their LC_{50} (Table 1)], (ii) decreased toxin ingestion by the bottom-feeding *A. aegypti* larvae be-

Table 1. Toxicity of soluble and crystalline Bti toxin to *Aedes aegypti* larvae. Crystals were prepared as described by Ang and Nickerson (*9*). The crystals (2 mg/ml) were solubilized overnight at 4°C in 0.05*M* NaOH (*p*H 11.7) containing 10 m*M* EDTA and were then centrifuged at 100,000*g* for 30 minutes (*10*). The solubilized supernatant proteins were adjusted to 25 times the desired bioassay concentration in 1 ml of 0.1*M* tris buffer (*p*H 7.4) and mixed with 10 μl of latex beads (0.8 μm, 10 percent solids; Sigma). After incubation at room temperature for 1 hour the beads were centrifuged at 15,000*g* for 10 minutes and the pellet was resuspended in 1 ml of tris containing 0.01 percent polyvinylpyrrolidone (*11*). Test solutions were diluted with 24 ml of deionized water for the bioassays. At least six dilutions of each toxin preparation were used; whenever latex beads were employed their final concentrations were identical. Values of LC_{50} were determined 4 hours after the addition of 10 to 20 larvae and are presented as means ± 2 standard errors. All the experiments were conducted with crystal toxin from a single purification (*12*). The LC_{50} values for crystals remained constant over at least a 10-month period.

Condition	*N**	LC_{50} (ng/ml)
Intact crystals	5	7.5 ± 1.6
Intact crystals mixed with latex beads	4	15.0 ± 2.6
Solubilized crystals	3	$5.3 \times 10^4 \pm 1.1 \times 10^3$
Solubilized crystals adsorbed to latex beads	6	190 ± 19.2

*Number of independent replications for each determination of LC_{50}.